scientific reports

Check for updates

OPEN

Pseudorapidity dependence of the bulk properties of hadronic medium in *pp* collisions at 7 TeV

Muhammad Ajaz[1], Abd Al Karim Haj Ismail[2,3]✉, Muhammad Waqas[4]✉, Mais Suleymanov[5], Atef AbdelKader[2,3] & Rustam Suleymanov[6]

The measured charged particle p_T spectra in proton-proton collisions obtained by the CMS experiment at CERN is compared with the simulation results of EPOS–LHC and Pythia8.24 models at 7 TeV center-of-mass energy. The Pythia8.24 model describes the experimental data very well, particularly in the high p_T region. The model also predicts the p_T spectra for $|\eta| < 2.4$ at $0 \leq p_T \leq 6$ GeV/c. The EPOS–LHC model underpredicts the p_T spectra from 0.1 to 2 GeV/c in all η bins for about 20% and the p_T spectrum from 0.1 to 4.2 GeV/c for $|\eta| < 2.4$ by about 15% while reasonably predicts well for $p_T >$ 4.2 GeV/c within the experimental errors. Furthermore, to get information about collective properties of the hadronic matter, modified Hagedorn function with embedded transverse flow velocity and thermodynamically consistent Tsallis distribution functions are used to fit the experimental data and simulated results. The values of χ^2/ndf show that the functions fit the data and simulation results well. The parameter extracted by the functions: β_T, T_0, and T_{eff} decreases with increasing η. The decrease in β_T with increasing η is due to the large energy deposition in lower rapidity bins producing rapid expansion due to large pressure gradient resulting quick expansion of the fireball. Similarly, large energy transfer in the lower pseudo-rapidity bin results in higher degree of excitation of the system which results larger values of T_0 and T_{eff}. The values of the fit constant N_0 increase with η where the values of N_0 extracted from Pythia8.24 are closer to the data than the EPOS–LHC model. The Pythia8.24 model has better prediction than the EPOS–LHC model which might be connected to its flow-like features and color re-connections resulting from different Parton interactions in the initial and final state.

High energy particle collision is a very complex topic that makes it hard to measure and understand the geometry, quantities, and global properties of the collisions. Therefore, in addition to the measurements of some quantities by experiments, one must rely on theoretical models to explain some other characteristics based on experimental results. Experiments using high energy *pp* collisions such as the Relativistic Heavy Ion Collider (RHIC)[1,2] and the Large Hadron Collider (LHC) have been very useful to study the characteristics of these collisions such as the flow effects, the pseudorapidity, and the transverse momentum distributions. On the other hand, different models have been presented in the literature which tried to describe the collision process at different stages[3,4].

A measurement of pseudorapidity density provides constraints to the modeling of the characteristics of *pp* collisions such as the direction of particle emission. The pseudorapidity (η) is given by $\eta = -\ln(\tan(\theta/2))$, where θ is the polar angle that the charged particles make with the anticlockwise beam direction. The presented analysis are of $dN_{ch}/d\eta$ and dN_{ch}/dp_T in a pseudorapidity range of $|\eta| < 2.4$ in steps of 0.2. In the current analysis, the charged hadrons (N_{ch}) includes decay products of particles with a lifetime of < 1 cm, while the products of secondary particles are excluded and a correction factor is applied for prompt leptons.

The p_T and η distributions of charged particles, pions, kaons, protons, and anti-protons produced in nucleus-nucleus, hadron-nucleus, and *pp* collisions are very important observables because they provide very crucial information about the anisotropy and dynamics of the final state particles produced in collisions at high energies. In addition, p_T spectra are different for different particles in the range of 0 to 100 GeV/c, which makes it difficult

[1]Department of physics, Abdul Wali Khan University Mardan, Mardan 23200, Pakistan. [2]College of Humanities and Sciences, Ajman University, Ajman 346, United Arab Emirates. [3]Nonlinear Dynamic Research Center (NDRC), Ajman University, Ajman 346, United Arab Emirates. [4]School of Nuclear Science and Technology, University of Chinese Academy of Sciences, Beijing 100049, China. [5]Baku State University, Baku, Azerbaijan. [6]Institute of Physics, National Academy of Sciences, Baku, Azerbaijan. ✉email: a.hajismail@ajman.ac.ae; waqas_phy313@ucas.ac.cn

to explain how wide is the distribution range for different energies. However, one can discuss different p_T ranges including very low, low, intermediate, high, and very high regions[5–10]. Generally, p_T spectra are the combination of two main processes, soft and hard processes. The soft processes are dominant at the low p_T range and the hard processes become more pronounced at higher p_T ranges. Furthermore, similar results are reported from predictions of different model simulations of the p_T distributions at different energies[11–14].

In this work, we contrasted the simulation results of the transverse momentum (p_T) distributions of the charged particles with the measurements of the experimental data in pp collisions at 7 TeV that are further analyzed by statistical functions to extract the bulk properties of the hadronic matter. The temperature at the kinetic freeze-out stage (T_0), the effective temperature (T_{eff}) and the average transverse flow velocity (β_T) are extracted by fitting the data with these statistical functions. T_0 and $< \beta_T >$ are obtained by using a modified Hagedorn function with embedded transverse flow velocity[15–18]. In addition, T_{eff} is extracted by using the Tsallis distribution function[19–23]. The experimental data are compared with the Monte Carlo models predictions elaborated in the following "Method and models" section. Fits explained in "Method and models" section is applied to the models' simulations as well as experimental data for better comparisons. It is worth mentioning that the error bars in the experimental data are the quadrature sum of systematic and statistical errors while in the case of models simulations only the statistical errors are shown. No error bars are used where fit curves are shown on data and model simulations.

The rest of this article is organized as follows: "Method and models" section presents an overview of the methods and Monte Carlo models' simulations under study. In "Results and discussion" section, the details of the analysis procedure, and the results of the simulations using EPOS[24] and Pythia[25] along with a comparison to experimental CMS data[26] and the fitting with theoretical functions, are presented. Finally, the summary and conclusions are given in "Summary and conclusion" section.

Method and models

Pseudorapidity (η) distributions in pp collisions at 7 TeV are obtained from the inner tracking system of the Compact Muon Solenoid experiment (CMS) at the Large Hadron Collider (LHC)[26] on March 30, 2010. The spectra obtained by the experiment were normalized to all non single diffractive events with corrections for trigger and selection efficiency, acceptance, and branching ratios. Simulations of two Monte Carlo models, EPOS[24] and Pythia[25] at the same energy are performed and are then compared with the measurements from the experimental data. These models are based on the simple Parton model using theory of Reggie-Gribov[27], which is a QCD based effective field theory that accounts for multiple interactions in parallel with Pomerons considered to represent the partons interactions[28]. A brief description about each of these models is provided below.

The generator EPOS[24] is a hadronic interaction Monte Carlo simulation package that is well known to simulate the hadronic interactions in high energy cosmic ray simulations. In addition, it is used to describe the minimum bias interactions and centrality dependence of heavy-ion collisions. EPOS is an acronym of Energy conserving quantum mechanical multiple scattering approach based on Partons Off-shell remnants and Splitting of parton ladders. Soft, semi-soft and hard Pomeron exchanges are used to describe the interaction between particles in EPOS, where the particle production originates from two kind of sources, cut Pomeron and remnant decays[29]. In its last improvement, EPOS was updated to a new version, called EPOS-LHC[24], to cover the energies of the LHC. The new version can reproduce all minimum bias results of all particles with transverse momentum from 0 to a few GeV/c. In addition, in case of very dense system in a small volume in pp collisions, a different parametrization of flow has been introduced in EPOS, compared to the large volume produced in heavy-ion collisions. In this paper, we have used the EPOS-LHC version of the EPOS model but for simplicity only EPOS will be used throughout the manuscript.

Pythia is one of the most widely used Monte Carlo event generator of particle collisions in high energy physics with emphasis on pp interactions[25]. The hadronization process of transforming the final outgoing coloured Partons into colourless particles is based on the Lund string fragmentation model[30]. The main event in a pp collision can be represented by a large number of processes, such as elastic and diffractive processes, electroweak processes, QCD hard and soft processes and top quark production. The model also implements the initial and final state radiations, multi Partonic interactions, beam remnants which are formed after the extraction of multi Partonic interactions[31]. We used Phythia8.24 version of the Pythia model but for simplicity we will be using Pythia throughout the manuscript. It is also pertinent to mention that one million events are simulated in case of both the models.

In a standard analysis, it is always important to compare the results of the simulation generated with the Monte Carlo models to experimental data. In addition to the comparison of models' prediction with the experimental data, we use the theoretical Hagedorn function[32] to fit the experimental data as well as the models' simulations to extract the freeze-out parameters. The Hagedorn function, a QCD -inspired inverse power law, which can produce the transverse mass m_T distribution of hadrons in pp and AA collisions. This Hagedorn function describes the bulk spectra in the low transverse mass region as well as the particles produced in QCD hard scatterings. The function is given as:

$$\frac{d^2N}{2\pi N_{ev} p_T dp_T dy} = C\left(1 + \frac{m_T}{p_0}\right)^{-n}. \tag{1}$$

Here, $m_t = \sqrt{p_T^2 + m_0^2}$ is the transverse mass of hadrons, m_0 the rest mass while C is the normalization constant. The n and p_0 in the equation are two free parameters of the function. Moreover, the Tsallis function[15–18] can excellently describe the p_T and m_T invariant distribution measured in pp collisions at high energies. There are several version of the Tsallis function that can give good fit results to the p_T spectra, however, the following

expression is a simple version of the Tsallis function[22] that describes the invariant spectra of particles in terms of the effective temperature T_{eff} and non-extensivity parameter q which accounts for the deviation of the p_T spectra from the usual Boltzmann–Gibbs exponential distribution function. This version of the Tsallis function is a consistent version of thermodynamics for the particle number, energy, density and pressure at mid-rapidity ($y \approx 0$), and is given by the following expression:

$$\frac{d^2N}{2\pi N_{ev} p_T dp_T dy} = C_q \left(1 + (q-1)\frac{m_T}{T_{eff}}\right)^{-1/(q-1)}. \tag{2}$$

where C_q is constant of the fit function, T_{eff} is the effective temperature, q is the non-extensive parameter and can also be considered as a measure of the non-thermalization[23]. When the parameter q is close to one, the thermalization degree of a system is larger and the Tsallis distribution approaches the normal Boltzmann–Gibbs exponential distribution function. On the other hand, the effective temperature parameter T_{eff} represents the contribution from the thermal motion of particles as well as the collective flow of expanding matter[22].

$$\frac{d^2N}{2\pi N_{ev} p_T dp_T dy} = C_q m_T \left(1 + (q-1)\frac{m_T}{T_{eff}}\right)^{-q/(q-1)}. \tag{3}$$

which is called the thermodynamically consistent Tsallis function throughout the paper or Tsallis function for shortness.

Assuming that $n = (q-1)^{-1}$ and $p_0 = nT$, we notice that Eqs. (1) and (2) are mathematically equivalent. One can see that the parameters n and q are inversely proportional to each other, as the value of the parameter n increases, the parameter q decreases.

$$\frac{d^2N}{2\pi N_{ev} p_T dp_T dy} = C\left(1 + \frac{m_T}{nT_0}\right)^{-n}. \tag{4}$$

Finally to include the transverse flow in Eq. (4), m_T is equated with

$$m_T = < \gamma_T > \left(m_T - p_T < \beta_T > \right). \tag{5}$$

These modifications have been discussed in[18,33,34] and have successfully calculated the average transverse flow velocity $< \beta_T >$ and T_0, and the equation is now known as the Hagedorn equation with embedded transverse flow velocity[35]:

$$\frac{d^2N}{2\pi N_{ev} p_T dp_T dy} = C\left(1 + < \gamma_T > \frac{m_T - p_T < \beta_T >}{nT_0}\right)^{-n}. \tag{6}$$

where C is the normalization constant and is to be normalized to 1. $< \gamma_t > = 1/\sqrt{1 - < \beta_t^2 >}$ and $< \beta_t >$ is the average transverse flow velocity. This simple form of the equation having a few parameters, is very powerful tool to compare different collisions with a small number of parameters. The Hagedorn function has reproduced the spectra described in[18,32,33] with physical parameters. We can re-arrange these terms in our current analysis as follows,

$$\frac{d^2N}{N_{ev} dp_T dy} = 2\pi p_T C\left(1 + < \gamma_T > \frac{m_T - p_T < \beta_T >}{nT_0}\right)^{-n}. \tag{7}$$

$$\frac{d^2N}{N_{ev} dp_T dy} = 2\pi C_q p_T m_T \left(1 + (q-1)\frac{m_T}{T_{eff}}\right)^{-q/(q-1)}. \tag{8}$$

The p_T spectra of charged hadrons from experiment as well as model simulations are fitted with Hagedorn equations (Eq. 7) and thermodynamically consistent Tsallis function (Eq. 8) to extract the fit parameters as explained above. We have used the method of least square for the extraction of the related parameters. The Tsallis function is very effective in providing an excellent description of the transverse momentum spectra of particles, for nucleus-nucleus (AA) as well as hadron-hadron (hh) collisions at high energies. The function has three free parameters including normalization/fitting constant indicating volume information, the non-extensivity parameter used to see the deviation of the distribution from the exponential Boltzman and Gibbs distribution, and the effective temperature which includes the flow information along with the thermal motion of the particles. Furthermore, to describe p_T distribution of particles in AA and hh collisions, different models with flow definitions are included in the Tsallis distribution function. Hagedorn function is one of them which among other parameters gives direct access to the transverse expansion (flow velocity) and kinetic freeze-out temperature with an excellent description of the p_T spectra at high energies. In addition, the modified Hagedorn function is very close to the ideal gas model. Both the Hagedorn and Tsallis models have the advantage that they cover a wide range of p_T due to the entropy parameter $q(n)$ where $q = 1/(n-1)$.

Results and discussion

The transverse momentum (p_T) spectra of charged hadrons simulated with the EPOS and Pythia models are compared with the pp collisions at $\sqrt{s} = 7$ TeV measured by the CMS experiment[26]. The initial conditions used for simulations are similar to that of experimental conditions. The p_T spectra from 0.1 to 2 GeV/c in different η bins from 0 to 2.4 in steps of 0.2, and the p_T spectrum from 0.1 to 6 GeV for $0 \leq \ \eta \ < 2.4$ as a single η bin are studied using the aforementioned models.

Figure 1 shows the p_T distributions of charged hadrons in different η bins starting from 0.1 (corresponding to $\eta = 0.0-0.2$) from top left to $\eta = 2.3$ (2.2−2.4) to the bottom right. The experimental data is shown by solid black markers while lines of different colors represent the two models calculations. A red solid line is used to show the results of the EPOS model, while the blue solid line is for Pythia results. The quadrature sum of the systematic and statistical errors are considered in the experimental results, while model calculations include the statistical errors only. The horizontal error bars show the bin size shown in the experimental results. The two event generators have the same horizontal bin size in p_T as the experimental data. It has been observed that for p_T above 0.8 GeV/c, Pythia measurements fully describe the p_T spectra at all the pseudorapidity regions. Below 0.3 GeV/c, Pythia model under-predicts the experimental data, while for $0.3 \leq p_T \leq 0.8$ GeV/c, the model slightly overshoot the experimental data which is about 10%. There is no significant η dependence observed in the model's predictions and have similar results for all pseudorapidity regions. The EPOS model under-predicts the experimental data over the entire p_T range up to about 20% and is also observed to be independent of all η regions understudy. The data to Monte Carlo ratio is shown in the lower panel of each plot which supports the above statement.

Figure 2 shows the predictions of the p_T spectra of the two models in comparison to the experimental data for $\eta \ < 2.4$ GeV/c. Again the Pythia model reproduced the experimental data over most of the p_T region within the experimental errors. For $p_T < 1$ GeV/c, the model slightly overshoot the data in a narrow region of the p_T for about 10%. The EPOS model again underestimates the experimental data over the entire p_T region with decreasing discrepancy with increasing p_T. The ratio of the Monte Carlo predictions to the data is also shown in the lower panel of the plot which supports our statements.

Figure 3 shows the η of charged hadrons integrated over the p_T for $-2.5 \leq \eta \leq 2.5$ in comparison with the models' predictions. Pythia model reproduced the experimental results of $dN_{ch}/d\eta$ very well for the whole η region, $-2.5 \leq \eta \leq 2.5$. The EPOS model does not reproduce the data and hence underpredicts the charged particles η integrated over p_T over the entire region of $-2.5 \leq \eta \leq 2.5$ from 10% to about 15%. The lower panel of the graph shows the ratio of the Monte Carlo predictions to the data. The description mentioned can easily be inferred from the ratio plot as well.

To extract the bulk properties of the hadronic matter created as a result of pp collisions at $\sqrt{s} = 7$ TeV, the CMS experimental data[36] and models' simulations are fitted with two statistical functions. The fit results of the data and two models' predictions are presented in Fig. 4 which show that the fit functions fit the data very well. The experimental data and model simulations are fitted by the modified Hagedorn function with embedded transverse flow velocity (Eq. 7) and thermodynamically consistent Tsallis distribution function (Eq. 8). Figure 4a,b show the p_T spectra of the experimental data in different η intervals fitted with the modified Tsallis and Hagedorn functions respectively. Similarly, Fig. 4c,d show the fit results of the two function on Pythia model's prediction while Fig. 4e,f show the fit results of the two statistical models on the EPOS model's predictions.

The spectra at different η intervals from 0 to 2.4 in steps of 0.2 respectively are scaled by 1, 2, 4, 8, 16, 32, 64, 128, 254, 512, 1024, and 2048 respectively for better visualisation. The values of the extracted parameters obtained from the fit by Hagedorn distribution function using Eq. (7) are listed in Table 1. *The values of* χ^2/ndf also show that the two functions fit the data and models' predictions very well given in the last column of the table. The values of transverse flow velocity (β_T), n, and Kinetic freeze-out temperature (T_0) are extracted by fitting the spectra of the experimental data and models' simulations tabulated as a third, fourth, and fifth column in the Table 1. These parameters are directly connected to the scattering centers involved in the interaction process.

The values of different parameters are extracted by fitting the experimental data and models' simulations in each η bin for better comparison of predictions with the measurements. The values of N_0, β_T, and T_0 decrease with η in data and both the models. The values of β_T and T_0 extracted by the fit functions from the EPOS model are closer to the experimental data than the Pythia model while opposite in the case for N_0 where the latter has similar values in Pythia with the data than the EPOS model.

In case of experimental data, the function described in Eq. (7) gives the value of $\beta_T = (0.3836 \pm 0.0002)$ c for $\eta = 0.1$, which corresponds to the η range from 0.0 to 0.2. The extracted value of $\beta_T = (0.3505 \pm 0.0002)$ c for the $\eta = 2.3$. In the case of Pythia model, the value of β_T varies from (0.6178 ± 0.0002) c for $\eta = 0.1$ to (0.593 ± 0.0002) c for $\eta = 2.3$, whereas it varies from (0.482 ± 0.0002) c to (0.347 ± 0.0002) c in case of EPOS model for the first and last regions of η. It has been observed that the variation in the value of β_T is monotonic in all the cases. The kinetic freeze–out temperature T_0, extracted by fitting the experimental data with Hagedorn function also shows a decreasing trend with increasing η starting from (76.37 ± 0.01) MeV at $\eta = 0.1$ to (71.86 ± 0.01) MeV at $\eta = 2.3$. The reason behind this decreasing trend of T_0 is the decrease of the energy transfer in the system due to the large penetration between participants particles as the system goes from mid-rapidity to the forward-rapidity region and this result is in agreement with our recent work[37]. A similar decreasing trend of the T_0 is observed by applying the fit function on the two models' predictions. In both of the cases, the value of T_0 decreases with increasing η. The highest and lowest values of T_0 for Pythia and EPOS models are (67.7 ± 0.02) MeV, (51.7 ± 0.02) MeV and (76.0 ± 0.02) MeV, (74.5 ± 0.01) MeV respectively.

The value of n obtained from the fitting function has also been observed to show a decreasing trend with increasing η. The decrease in the values of n in case of experimental data is clearer than the data and EPOS model where slight variation in the values of n are observed. Furthermore, the values of n for EPOS model are closer

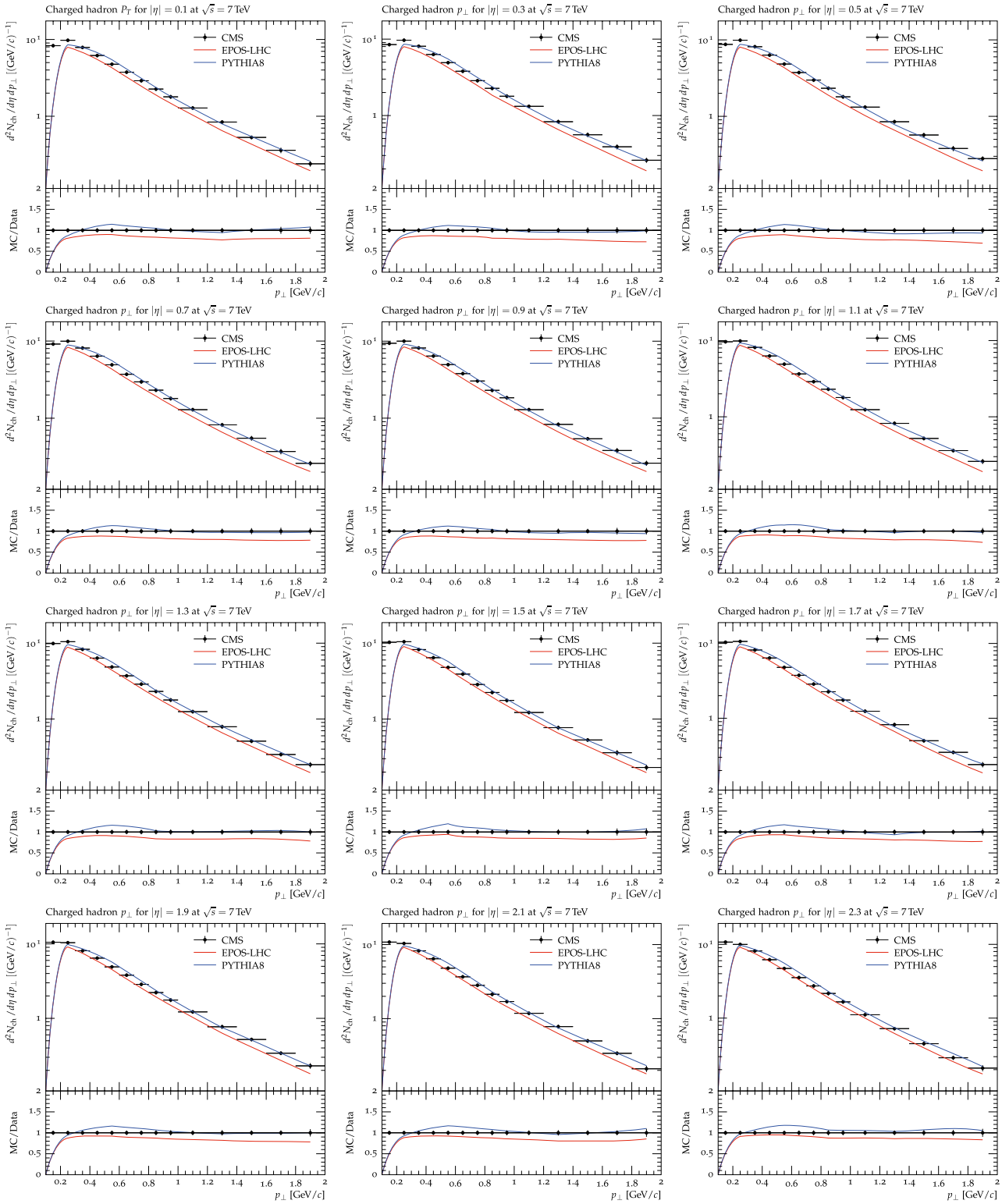

Figure 1. The p_T spectra of all charged hadrons are presented at different pseudorapidity bins measured by the CMS experiment in comparison with the prediction of EPOS and Pythia models. Black solid markers represent the experimental measurements while lines of different colors show the models' predictions. Blue line shows the Pythia while the red line is used for the EPOS model's prediction.

to the experimental data than the Pythia model which has higher values in all the cases of different η intervals. Lastly, the values of normalization constant, N_0, shows an increasing trend with increasing η intervals in data as

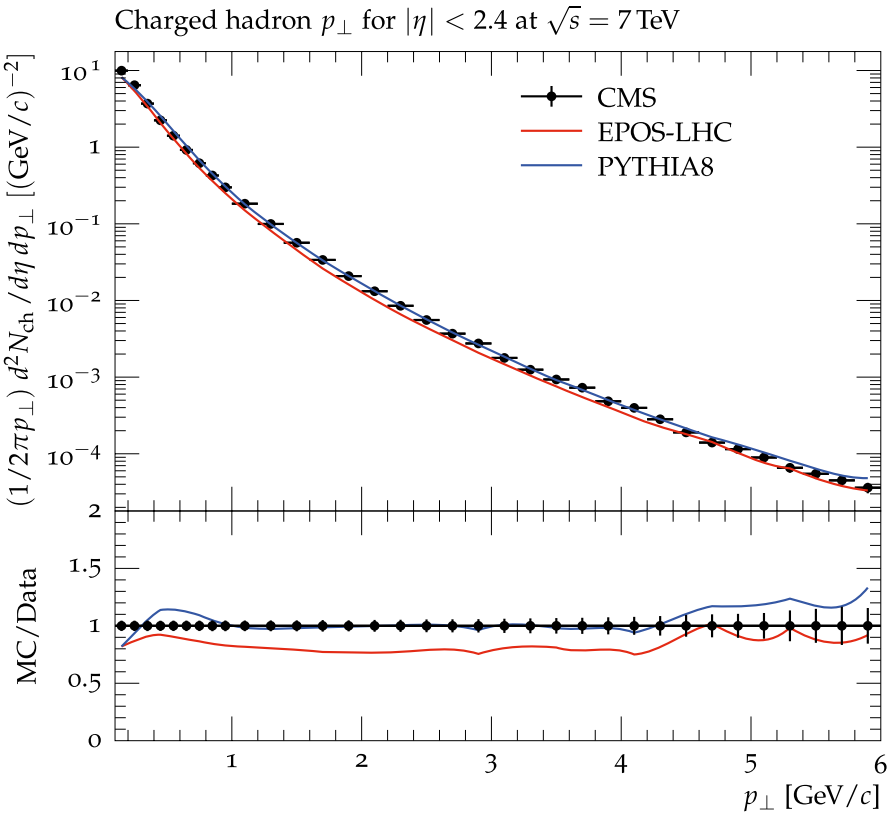

Figure 2. The p_T spectrum of charged hadrons at η < 2.4 measured by the CMS experiment compared with the prediction of the EPOS and Pythia models. Solid black markers represents the experimental measurements while lines of different colors show the models' predictions. A blue line shows the Pythia prediction while the red line represents the EPOS model predictions.

well as in both of the models. It increases from 92.8 ± 0.1 to 96.0 ± 0.1 in data while from 88.0 ± 0.1 to 96.5 ± 0.1 and 78.0 ± 0.1 to 86.0 ± 0.1 in Pythia and EPOS models respectively.

The values of different parameter obtained by fitting the experimental data and models' simulations by thermodynamically consistent Tsallis function are given in Table 2. These parameters include the effective temperature (T_{eff}), non-extensivity parameter q and normalization constant N_0 for different values of η from 0 to 2.4 in steps of 0.2. The values of T_{eff} decreases with η monotonically in experimental data and in both of the models. It varies from (81.93 ± 0.02) MeV to (69.46 ± 0.02) MeV in case of data and from (108.24 ± 0.02) MeV to (94.75 ± 0.02) MeV and (97.26 ± 0.02) MeV to (81.38 ± 0.02) MeV in cases of Pythia and EPOS models respectively. For a particular η bin, both models have higher values of T_{eff} with EPOS has closer value than the Pythia model. The value of q has again a monotonically increasing behavior with η but now both the models have lower values of q than the data. Again the values of q in the case of EPOS model has closer values than the Pythia model. The values of q varies from 1.185 ± 0.002 to 1.192 ± 0.002 in case of experimental data, from 1.140 ± 0.002 to 1.148 ± 0.002 in case of Pythia model whereas from 1.150 ± 0.002 to 1.167 ± 0.002 in the case of EPOS model.

The relation of q with n can be established by comparing the two tables resulting from two different functions. A slight variation in q yields an appreciable inverse variation in the value of n. It has resulted from this study that the n parameter decreases while the q increases with η.

An increasing trend is observed in the values of N_0 with increasing η extracted by the fit using Tsallis function. The value varies from 93.0 ± 0.2 to 97.1 ± 0.2 in case of experimental data while for Pythia it yields 88.8 ± 0.2 for $\eta = 0.1$ while 98.4 ± 0.2 for $\eta = 2.3$. The function yield a value of 77.2 ± 0.2 for the lower η bin while 86.3 ± 0.2 for the higher η bin. The values of N_0 in case of the Pythia model is closer to the experimental data than the EPOS model. Since N_0 is proportional to the multiplicity of particles and Pythia reproduced similar multiplicity hence predicted better results than the EPOS model. This might be connected to the effects that are incorporated in the Pythia model such as flow-like effect and color reconnection effect which is produced from simultaneous hard sub-collisions forming color strings between initial and final state partons from separate hard scatterings due to which the model predicts the data well.

Before going to conclusion section we would like to clarify that the T_0 and $T_e eff$ are not different. The former does not include the flow effect, however the later includes the flow effect. We observed that both of them decrease with increasing pseudo-rapidity due to the large energy transfer in lower pseudo-rapidity intervals. The physics behind this is that larger energy transfer in the lower pseudo-rapidity bin results in higher degree of excitation of the system which results in larger T_0 and T_{eff}[10,38–41] and this indicates that the system in lower pseudo-rapidity

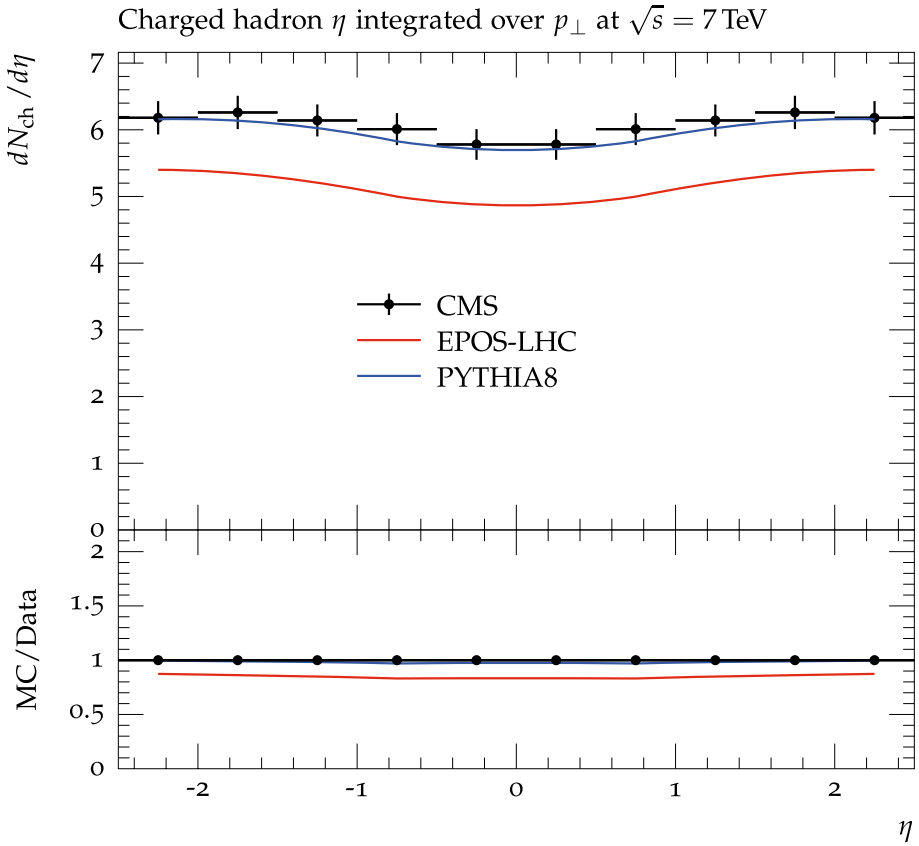

Figure 3. The charged hadrons η integrated over p_T at $-2.5 \leq \eta \leq 2.5$ measured by the CMS experiment is compared with the predictions of the EPOS and Pythia models. Solid black markers represent the experimental measurements while lines of different colors show the models' predictions. A red line shows the Pythia's predictions while the blue line represents the EPOS model predictions.

intervals comes to equilibrium quickly. In addition we also observed that q (n) is increasing (decreasing) with the increase of rapidity. As discussed above, q and n are reciprocal. A system with smaller q (more closer to unity) and larger n indicates to be more closer to equilibrium state[42–45]. In the present work the increase (decrease) of q (n) with increasing η claims that the system goes far from the equilibrium state as the psuedo-rapidity intervals is larger. The β_T is also observed to decrease with increasing η due to large energy deposition in lower rapidity bins. Actually, the large deposition of energy in a system indicates its rapid expansion. In the present work, the larger β_T in lower η bins shows that there is large pressure gradient due to the fact that large amount of energy is transferred to the system which results in a quick expansion of the fireball.

Summary and conclusion

Simulations of EPOS and Pythia models are performed and then compared with the measurements of the CMS experimental data in pp collisions at $\sqrt{s} = 7$ TeV. The transverse-momentum (p_T) spectra are presented from 0.1 to 2 GeV/c in twelve pseudorapidity (η) intervals from 0 to 2.4 in steps of 0.2 and the p_T spectrum from 0.1 to 6 GeV/c for a wider η interval, $0 \leq \eta \leq 2.4$ as a single bin. The Pythia model predicts the p_T spectra at all the pseudorapidity bins very well particularly at the higher value of p_T, while over predicts the distribution slightly at the lower p_T region. The model also predicts the p_T spectra for a wider range of η, $\eta < 2.4$ and over a wide range of p_T, $0 \leq p_T \leq 6$ GeV/c. However, within the experimental error a slight bump is predicted in a narrow region at lower p_T interval. The EPOS model under-predicts the p_T spectra over the entire p_T range and in all η intervals. The model also underestimates the experimental results of p_T spectra for all η intervals for about 15% at $\eta < 2.4$ while a reasonable agreement is shown for $p_T > 4.2$ GeV/c within the experimental errors. The Pythia model reproduce the charged particle pseudorapidity integrated over p_T for the whole region of η, $-2.5 \leq \eta \leq 2.5$ very well whereas the EPOS model under-predicts from 10% to about 15%.

Furthermore, the models' predictions and the experimental data are fitted by two statistical functions to get information about some collective properties of the hadronic matter. The measured experimental data and models simulations are fitted by modified Hagedorn function with embedded transverse flow velocity and thermodynamically consistent Tsallis distribution function. The two function fitted the data and models prediction very well. The values of transverse flow velocity (β_T), and Kinetic freeze–out temperature (T_0) extracted from the Hagedorn distribution function while effective temperature (T_{eff}) is obtained from the Tsallis function. The value of β_T, T_0, and T_{eff} decrease with increasing η because large energy transfer in the lower pseudo-rapidity bin results in higher degree of excitation of the system which results larger values of T_0 and/or T_{eff}. Furthermore,

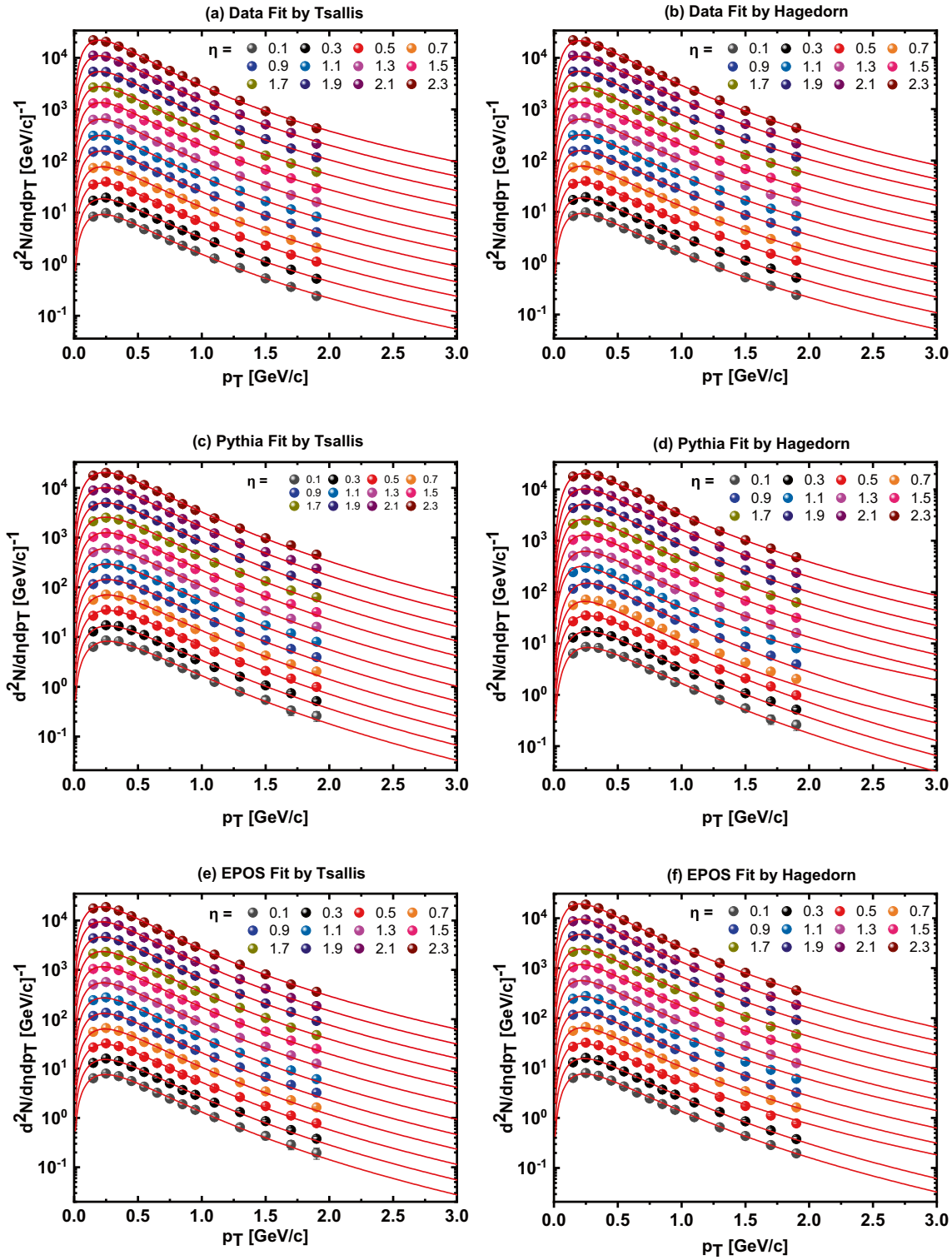

Figure 4. The charged hadrons p_T spectra in different η intervals from 0 to 2.4 in steps of 0.2 measured by the CMS experiment is fitted with the Tsallis function (Eq. 7) (left) and Hagedorn function (Eq. 8) (right) shown in the first row (**a** and **b**). Same markers with different colors are used to represent each slice of η bin. Lines of the same color are used to show the fit results on the experimental data. The second (**c** and **d**) and third (**e** and **f**) rows show the Pythia and EPOS simulations fitted with the Tsallis (left) and Hagedorn (right) functions, respectively.

Model	η	N_0	$\beta_T(GeV/c)$	n	$T_0(MeV)$	χ^2/ndf
CMS data	0.0–0.2	92.8 ± 0.1	0.3836 ± 0.0002	5.749 ± 0.001	76.37 ± 0.01	3.9416/11
	0.2–0.4	94.0 ± 0.1	0.3979 ± 0.0002	5.749 ± 0.001	75.85 ± 0.01	2.8339/11
	0.4–0.6	95.0 ± 0.1	0.3990 ± 0.0002	5.738 ± 0.001	75.45 ± 0.01	4.3806/11
	0.6–0.8	96.0 ± 0.1	0.3767 ± 0.0002	5.738 ± 0.001	76.12 ± 0.01	2.6043/11
	0.8–1.0	96.8 ± 0.2	0.3765 ± 0.0002	5.736 ± 0.001	76.18 ± 0.01	2.7891/11
	1.0–1.2	96.4 ± 0.2	0.3602 ± 0.0002	5.702 ± 0.001	76.23 ± 0.01	3.9972/11
	1.2–1.4	97.5 ± 0.1	0.3420 ± 0.0002	5.545 ± 0.001	76.25 ± 0.01	1.9827/11
	1.4–1.6	98.1 ± 0.1	0.3281 ± 0.0002	5.690 ± 0.002	76.28 ± 0.01	5.0891/11
	1.6–1.8	99.5 ± 0.1	0.3260 ± 0.0002	5.538 ± 0.002	73.45 ± 0.01	5.5269/11
	1.8–2.0	99.8 ± 0.1	0.3220 ± 0.0002	5.538 ± 0.002	73.25 ± 0.01	4.3067/11
	2.0–2.2	98.0 ± 0.2	0.3490 ± 0.0002	5.875 ± 0.012	74.66 ± 0.01	9.4020/11
	2.2–2.4	96.0 ± 0.1	0.3505 ± 0.0002	5.84 ± 0.012	71.86 ± 0.01	6.8266/11
Pythia model	0.0–0.2	88.0 ± 0.1	0.6178 ± 0.0002	7.529 ± 0.002	67.7 ± 0.02	3.3603/11
	0.2–0.4	90.0 ± 0.1	0.6166 ± 0.0002	7.510 ± 0.002	67.5 ± 0.02	3.3568/11
	0.4–0.6	90.5 ± 0.1	0.6116 ± 0.0002	7.507 ± 0.002	67.5 ± 0.02	2.3721/11
	0.6–0.8	80.5 ± 0.1	0.5876 ± 0.0002	6.057 ± 0.002	54.5 ± 0.02	1.6427/11
	0.8–1.0	93.0 ± 0.1	0.6704 ± 0.0002	6.808 ± 0.002	51.8 ± 0.02	1.4146/11
	1.0–1.2	95.0 ± 0.1	0.510 ± 0.0022	5.101 ± 0.121	51.8 ± 0.02	5.1238/11
	1.2–1.4	96.5 ± 0.1	0.610 ± 0.0002	5.912 ± 0.002	51.9 ± 0.02	1.3226/11
	1.4–1.6	97.0 ± 0.1	0.604 ± 0.0002	5.912 ± 0.001	52.1 ± 0.01	1.7307/11
	1.6–1.8	97.5 ± 0.1	0.601 ± 0.0002	5.945 ± 0.001	52.0 ± 0.01	1.1803/11
	1.8–2.0	97.5 ± 0.1	0.600 ± 0.0002	5.945 ± 0.001	51.7 ± 0.02	1.3284/11
	2.0–2.2	97.0 ± 0.1	0.598 ± 0.0002	5.945 ± 0.001	51.7 ± 0.01	1.8547/11
	2.2–2.4	96.5 ± 0.1	0.593 ± 0.0002	5.945 ± 0.001	51.7 ± 0.02	1.2900/11
EPOS-LHC model	0.0–0.2	78.0 ± 0.1	0.482 ± 0.0002	6.678 ± 0.001	76.0 ± 0.02	2.4992/11
	0.2–0.4	77.5 ± 0.1	0.467 ± 0.0002	6.678 ± 0.001	75.9 ± 0.01	1.8971/11
	0.4–0.6	95.0 ± 0.2	0.417 ± 0.0002	5.77 ± 0.001	74.5 ± 0.02	5.1725/11
	0.6–0.8	79.0 ± 0.2	0.415 ± 0.0002	5.98 ± 0.002	74.5 ± 0.02	2.3327/11
	0.8–1.0	81.5 ± 0.1	0.406 ± 0.0002	5.98 ± 0.002	74.5 ± 0.02	1.2255/11
	1.0–1.2	96.0 ± 0.1	0.389 ± 0.0002	5.79 ± 0.001	74.5 ± 0.02	5.7511/11
	1.2–1.4	84.0 ± 0.1	0.381 ± 0.0002	5.99 ± 0.001	74.5 ± 0.02	0.8810/11
	1.4–1.6	85.0 ± 0.1	0.377 ± 0.0002	5.99 ± 0.001	74.5 ± 0.01	0.7250/11
	1.6–1.8	86.0 ± 0.1	0.369 ± 0.0002	5.99 ± 0.001	74.5 ± 0.02	0.6412/11
	1.8–2.0	86.0 ± 0.1	0.362 ± 0.0002	5.99 ± 0.001	74.5 ± 0.01	0.2543/11
	2.0–2.2	86.5 ± 0.1	0.353 ± 0.0002	5.996 ± 0.001	74.5 ± 0.01	0.6915/11
	2.2–2.4	86.0 ± 0.1	0.347 ± 0.0002	6.081 ± 0.002	74.5 ± 0.01	0.6222/11

Table 1. The values of free parameters (T_0 and β_T), normalization constant (N_0), n, and χ^2/ndf at different η values from 0 to 2.4 in steps of 0.2 using modified Hagedorn function with embedded transverse flow velocity using Eq. (7) for the CMS data, Pythia model, and EPOS model.

the decrease in β_T with increasing η is due to the large energy deposition in lower rapidity bins producing rapid expansion. In the present work, the larger β_T in lower η bins shows that there is large pressure gradient due to the fact that large amount of energy is transferred to the system resulting in a quick expansion of the fireball. It is concluded that the Pythia model describes the experimental data at most of the p_T regions for all the η bins, while the EPOS underpredicts mostly. The Pythia model also predicted the p_T distribution over a wider p_T range well which might be connected to the color re-connection and flow-like feature of the Pythia model, whereas the EPOS reproduced the distribution at higher values of the p_T only and largely underpredicts the distribution. Although, the models under-study reproduced the p_T distribution of the charged particles in some region of p_T in different η regions presented from 0 to 2.4 in steps of 0.2, but none of them completely describe all the distribution over the entire p_T range.

Model	η	N_0	q	$T_{eff}\,(MeV)$	χ^2/ndf
CMS fata	0.0–0.2	93.0 ± 0.2	1.185 ± 0.002	81.93 ± 0.02	4.7095/11
	0.2–0.4	94.1 ± 0.2	1.187 ± 0.002	82.09 ± 0.02	2.9418/11
	0.4–0.6	95.2 ± 0.2	1.187 ± 0.001	82.17 ± 0.02	4.2392/11
	0.6–0.8	96.1 ± 0.2	1.187 ± 0.001	80.16 ± 0.02	2.9714/11
	0.8–1.0	96.9 ± 0.2	1.188 ± 0.001	79.17 ± 0.02	2.9565/11
	1.0–1.2	96.0 ± 0.3	1.189 ± 0.002	77.57 ± 0.02	3.8693/11
	1.2–1.4	97.2 ± 0.2	1.189 ± 0.002	75.69 ± 0.02	4.8091/11
	1.4–1.6	98.4 ± 0.2	1.189 ± 0.002	75.45 ± 0.02	5.8391/11
	1.6–1.8	99.2 ± 0.2	1.189 ± 0.033	74.05 ± 0.02	6.7898/11
	1.8–2.0	99.3 ± 0.2	1.190 ± 0.001	73.55 ± 0.02	5.3094/11
	2.0–2.2	99.4 ± 0.2	1.190 ± 0.003	72.06 ± 0.02	6.7880/11
	2.2–2.4	97.1 ± 0.2	1.192 ± 0.002	69.46 ± 0.02	6.4629/11
Pythia model	0.0–0.2	88.8 ± 0.2	1.140 ± 0.002	108.24 ± 0.2	4.4459/11
	0.2–0.4	90.4 ± 0.2	1.140 ± 0.002	107.94 ± 0.02	4.5186/11
	0.4–0.6	91.4 ± 0.2	1.140 ± 0.002	106.84 ± 0.02	3.3732/11
	0.6–0.8	92.7 ± 0.2	1.140 ± 0.002	105.83 ± 0.02	2.8549/11
	0.8–1.0	94.1 ± 0.2	1.142 ± 0.002	103.75 ± 0.02	2.7462/11
	1.0–1.2	95.7 ± 0.2	1.142 ± 0.002	102.73 ± 0.02	2.5065/11
	1.2–1.4	97.0 ± 0.2	1.146 ± 0.002	100.00 ± 0.02	2.0923/11
	1.4–1.6	97.5 ± 0.2	1.144 ± 0.002	100.00 ± 0.02	2.3008/11
	1.6–1.8	98.1 ± 0.2	1.146 ± 0.002	97.70 ± 0.02	1.6759/11
	1.8–2.0	98.2 ± 0.2	1.147 ± 0.002	96.95 ± 0.02	1.1737/11
	2.0–2.2	98.2 ± 0.2	1.148 ± 0.002	95.58 ± 0.02	1.5751/11
	2.2–2.4	98.4 ± 0.2	1.148 ± 0.002	94.75 ± 0.02	1.4281/11
EPOS-LHC model	0.0–0.2	77.2 ± 0.2	1.150 ± 0.002	97.26 ± 0.02	2.5239/11
	0.2–0.4	77.4 ± 0.2	1.151 ± 0.002	96.28 ± 0.02	2.4604/11
	0.4–0.6	78.2 ± 0.2	1.153 ± 0.002	95.04 ± 0.02	1.8541/11
	0.6–0.8	79.6 ± 0.2	1.154 ± 0.002	94.12 ± 0.02	2.5161/11
	0.8–1.0	80.8 ± 0.2	1.156 ± 0.002	91.41 ± 0.02	2.3710/11
	1.0–1.2	82.5 ± 0.2	1.158 ± 0.002	89.46 ± 0.02	1.5124/11
	1.2–1.4	83.3 ± 0.2	1.161 ± 0.002	88.11 ± 0.02	1.8027/11
	1.4–1.6	84.8 ± 0.2	1.163 ± 0.002	86.25 ± 0.02	1.6193/11
	1.6–1.8	85.6 ± 0.2	1.164 ± 0.002	85.15 ± 0.02	1.0484/11
	1.8–2.0	86.1 ± 0.2	1.165 ± 0.002	84.13 ± 0.02	0.9275/11
	2.0–2.2	86.2 ± 0.2	1.166 ± 0.002	82.32 ± 0.02	0.7033/11
	2.2–2.4	86.3 ± 0.2	1.167 ± 0.002	81.38 ± 0.02	0.4957/11

Table 2. The values of free parameters (q and T_{eff}), normalization constant (N_0), and χ^2/ndf at different values of η from 0 to 2.4 in steps of 0.2 using thermodynamically consistent Tsallis distribution function given by Eq. (8) are shown here for the experimental data, Pythia model, and EPOS model.

Received: 4 January 2022; Accepted: 22 April 2022

References

1. Back, B. *et al.* Charged-particle pseudorapidity density distributions from au+au collisions at $\sqrt{s_{NN}} = 130$ gev. *Phys. Rev. Lett.* **87**, 102303–102303. https://doi.org/10.1103/PhysRevLett.87.102303 (2001).
2. Bearden, I. *et al.* Charged particle densities from au + au collisions at $\sqrt{s_{NN}} = 130$ gev. *Phys. Lett. B* **523**, 227–233. https://doi.org/10.1016/S0370-2693(01)01333-8 (2001).
3. Liu, Y., Ko, C. & Song, T. Hot medium effects on j/ψ production in $p + pb$ collisions at $\sqrt{s_{NN}} = 5.02$ TeV. *Phys. Lett. B*https://doi.org/10.1016/j.physletb.2013.12.016 *(2013).*
4. Akkelin, S. V. & Sinyukov, Y. M. Entanglement of scales as a possible mechanism for decoherence and thermalization in relativistic heavy ion collisions. *Phys. Rev. C* **89**, 034910. https://doi.org/10.1103/PhysRevC.89.034910 (2014).
5. Ullah, S. *et al.* Hadron production models prediction for p_T distribution of charged hadrons in pp interactions at 7 TeV. *Sci. Rep.* **9**, 11811. https://doi.org/10.1038/s41598-019-48272-4 (2019).
6. Waqas, M. & Liu, F.-H. Centrality dependence of kinetic freeze-out temperature and transverse flow velocity in high energy nuclear collisions. *Indian J. Phys.*https://doi.org/10.1007/s12648-021-02058-5 *(2021).*
7. Ajaz, M. *et al.* Centrality dependence of P_T distributions and nuclear modification factor of charged particles in Pb-Pb interactions at $\sqrt{S_{NN}} = 2.76$ TeV. *Results Phys.* **30**, 104790. https://doi.org/10.1016/j.rinp.2021.104790 (2021).

8. Haj Ismail, A. Monte Carlo simulation of the cosmic muon charge ratio. *Kuwait J. Sci.* **49**, 1–8. https://doi.org/10.48129/kjs.v49i1.11497 (2022).
9. Ajaz, M. *et al.* Study of pT spectra of light particles using modified Hagedorn function and cosmic rays Monte Carlo event generators in proton-proton collisions at 900 GeV center of mass energy. *Eur. Phys. J. Plus.* **2022**(137), 1–9. https://doi.org/10.1140/epjp/s13360-021-02271-5 (2022).
10. Waqas, M., Peng, G. X., Wang, R.-Q., Ajaz, M. & Haj Ismail, A. A. K. Freezeout properties of different light nuclei at the RHIC Beam Energy Scan. *Eur. Phys. J. Plus* **136**, 1082. https://doi.org/10.1140/epjp/s13360-021-02089-1 (2021).
11. Ajaz, M., Khan, R., Wazir, Z., Khan, I. & Bibi, T. Model prediction of transverse momentum spectra of strange hadrons in *pp* collisions at $\sqrt{s} = 200$ GeV. *Int. J. Theor. Phys.* **59**, 3338–3347. https://doi.org/10.1007/s10773-020-04584-0 (2020).
12. Ajaz, M., Tufail, M. & Ali, Y. Study of the production of strange particles in proton-proton collisions at $\sqrt{S} = 0.9$ TeV. *Arab. J. Sci. Eng.* **45**, 411. https://doi.org/10.1007/s13369-019-04224-8 (2020).
13. Khan, R. & Ajaz, M. Model predictions of charge particle densities and multiplicities in the forward region at 7 TeV. *Mod. Phys. Lett. A* **35**, 2050190. https://doi.org/10.1142/S0217732320501904 (2020).
14. Ajaz, M., Khan, R., Ali, Y. & Suleymanov, M. K. Testing of model predictions of forward energy flow in *pp* collisions at $\sqrt{s} = 7$ TeV. *Mod. Phys. Lett. A* **35**, 1950349. https://doi.org/10.1142/S0217732319503498 (2019).
15. Olimov, K. K. *et al.* Multiplicity dependencies of midrapidity transverse momentum spectra of identified charged particles in $p + p$ collisions at $(s)^{1/2} = 13$ TeV at LHC. *Int. J. Mod. Phys. A* **36**, 2150149. https://doi.org/10.1142/S0217751X21501499 (2021).
16. Olimov, K. K., Iqbal, A. & Masood, S. Systematic analysis of midrapidity transverse momentum spectra of identified charged particles in $p + p$ collisions at $(s_{nn})^{1/2} = 2.76$, 5.02, and 7 TeV at the LHC. *Int. J. Mod. Phys. A* **35**, 2050167. https://doi.org/10.1142/S0217751X20501675 (2020).
17. Khandai, P. K., Sett, P., Shukla, P. & Singh, V. System size dependence of hadron p_T spectra in p+p and Au+Au collisions at $\sqrt{s_{NN}} = 200$ GeV. *J. Phys. G* **41**, 025105. https://doi.org/10.1088/0954-3899/41/2/025105 (2014).
18. Olimov, K. K. *et al.* Combined analysis of midrapidity transverse momentum spectra of the charged pions and kaons, protons and antiprotons in $p + p$ and Pb+Pb collisions at $(s_{nn})^{1/2} = 2.76$ and 5.02 TeV at the LHC. *Mod. Phys. Lett. A* **35**, 2050237. https://doi.org/10.1142/S0217732320502375 (2020).
19. Adare, A. *et al.* Measurement of neutral mesons in p+p collisions at $\sqrt{s}$= 200 GeV and scaling properties of hadron production. *Phys. Rev. D* **83**, 052004. https://doi.org/10.1103/PhysRevD.83.052004 (2011).
20. Cleymans, J. *et al.* Systematic properties of the Tsallis distribution: Energy dependence of parameters in high-energy p-p collisions. *Phys. Lett. B* **723**, 351–354. https://doi.org/10.1016/j.physletb.2013.05.029 (2013).
21. Khandai, P. K., Sett, P., Shukla, P. & Singh, V. Hadron spectra in p+p collisions at RHIC and LHC energies. *Int. J. Mod. Phys. A* **28**, 1350066. https://doi.org/10.1142/S0217751X13500668 (2013).
22. Cleymans, J. & Worku, D. The Tsallis distribution in proton-proton collisions at $\sqrt{s} = 0.9$ TeV at the LHC. *J. Phys. G* **39**, 025006. https://doi.org/10.1088/0954-3899/39/2/025006 (2012).
23. Wilk, G. & Wlodarczyk, Z. On the interpretation of nonextensive parameter q in Tsallis statistics and Levy distributions. *Phys. Rev. Lett.* **84**, 2770. https://doi.org/10.1103/PhysRevLett.84.2770 (2000).
24. Pierog, T., Karpenko, I., Katzy, J. M., Yatsenko, E. & Werner, K. EPOS LHC: Test of collective hadronization with data measured at the CERN Large Hadron Collider. *Phys. Rev. C* **92**, 034906. https://doi.org/10.1103/PhysRevC.92.034906 (2015).
25. Sjostrand, T., Mrenna, S. & Skands, P. Z. PYTHIA 6.4 physics and manual. *JHEP* **05**, 026. https://doi.org/10.1088/1126-6708/2006/05/026 (2006).
26. Khachatryan, V. *et al.* Transverse-momentum and pseudorapidity distributions of charged hadrons in *pp* collisions at $\sqrt{s} = 7$ TeV. *Phys. Rev. Lett.* **105**, 022002. https://doi.org/10.1103/PhysRevLett.105.022002 (2010).
27. Drescher, H., Hladik, M., Ostapchenko, S., Pierog, T. & Werner, K. Parton-based Gribov-Regge theory. *Phys. Rep.* **350**, 93–289. https://doi.org/10.1016/S0370-1573(00)00122-8 (2001).
28. Drescher, H. J., Hladik, M., Ostapchenko, S., Pierog, T. & Werner, K. Parton based Gribov-Regge theory. *Phys. Rep.* **350**, 93–289. https://doi.org/10.1016/S0370-1573(00)00122-8 (2001).
29. Pierog, T. & Werner, K. Epos model and ultra high energy cosmic rays. *Nucl. Phys. B Proc. Suppl.* **196**, 102–105. https://doi.org/10.1016/j.nuclphysbps.2009.09.017 (2009).
30. Andersson, B., Gustafson, G., Ingelman, G. & Sjöstrand, T. Parton fragmentation and string dynamics. *Phys. Rep.* **97**, 31–145. https://doi.org/10.1016/0370-1573(83)90080-7 (1983).
31. Sjöstrand, T. *et al.* An introduction to pythia 8.2. *Comput. Phys. Commun.* **191**, 159–177. https://doi.org/10.1016/j.cpc.2015.01.024 (2015).
32. Hagedorn, R. Multiplicities, p_T distributions and the expected hadron → quark-gluon phase transition. *La Rivista del Nuovo Cimento* **1978–1999**(6), 1–50 (1983).
33. Kaidalov, A. B. & Ter-Martirosian, K. A. Multiple production of hadrons at high-energies in the model of quark-gluon strings. *Sov. J. Nucl. Phys.* **39**, 979 (1984).
34. Waqas, M. *et al.* Decoupling of non-strange, strange and multi-strange particles from the system in Cu–Cu, Au–Au and Pb–Pb collisions at high energies. *Chin. J. Phys.* **77**, 1713-1722. https://doi.org/10.1016/j.cjph.2022.03.034 (2022).
35. Waqas, M., Liu, F.-H., Li, L.-L. & Alfanda, H. M. Effective (kinetic freeze-out) temperature, transverse flow velocity and kinetic freeze-out volume in high energy collisions. *Nucl. Sci. Tech.* **31**, 109. https://doi.org/10.1007/s41365-020-00821-7 (2020). arxiv:2001.06796.
36. Khachatryan, V. *et al.* Transverse-momentum and pseudorapidity distributions of charged hadrons in pp collisions at $\sqrt{s} = 0.9$ and 2.36 tev. *J. High Energy Phys.* **41**, 1029–8479. https://doi.org/10.1007/JHEP02(2010)041 (2010).
37. Waqas, M. *et al.* Study of kinetic freeze-out parameters as a function of rapidity in pp collisions at CERN SPS energies. *Entropy* **23**, 1363. https://doi.org/10.3390/e23101363 (2021).
38. Waqas, M. *et al.* Extraction of freezeout parameters and their dependence on collision energy and collision cross-section (2021). arxiv:2112.00975.
39. Waqas, M., Peng, G.-X., Liu, F.-H. & Wazir, Z. Effects of coalescence and isospin symmetry on the freezeout of light nuclei and their anti-particles. *Sci. Rep.* **11**, 20252. https://doi.org/10.1038/s41598-021-99455-x (2021).
40. Yang, P.-P., Ajaz, M., Waqas, M., Liu, F.-H. & Suleymanov, M. Pseudorapidity dependence of the p_t spectra of charged hadrons in *pp* collisions at $\sqrt{s} = 0.9$ and 2.36 tev. *J. Phys. G Nucl. Part. Phys.*http://iopscience.iop.org/article/10.1088/1361-6471/ac5d0b *(2022).*
41. Waqas, M., Haj Ismail, A. A. K., Ajaz, M. & AbdelKader, A. Excitation function of kinetic freeze-out parameters at 6.3, 17.3, 31, 900 and 7000 GeV. *Universe* **8**, 138. https://doi.org/10.3390/universe8020138 (2022).
42. Waqas, M., Peng, G. X. & Liu, F.-H. An evidence of triple kinetic freezeout scenario observed in all centrality intervals in Cu-Cu, Au-Au and Pb-Pb collisions at high energies. *J. Phys. G Nucl. Part. Phys.* **48**, 075108 https://doi.org/10.1088/1361-6471/abdd8d (2021).
43. Waqas, Muhammad, Liu, Fu.-Hu., Wang, Rui-Qin. & Siddique, Irfan. Energy scan/dependence of kinetic freeze-out scenarios of multi-strange and other identified particles in central nucleus-nucleus collisions. *Eur. Phys. J. A* **56**, 188. https://doi.org/10.1140/epja/s10050-020-00192-y (2020).
44. Li, L.-L., Liu, F.-H., Waqas, M. & Ajaz, M. Analyzing transverse momentum spectra by a new method in high-energy collisions. *Universe* **8**, 31. https://doi.org/10.3390/universe8010031 (2022).

45. Li, L.-L., Liu, F.-H. & Olimov, K. K. Excitation functions of Tsallis-like parameters in high-energy nucleus-nucleus collisions. *Entropy* **23**, 478. https://doi.org/10.3390/e23040478 (2021).

Acknowledgements
The authors would like to acknowledge Abdul Wali Khan University Mardan for providing all possible facilities and the support of Ajman University Internal Research Grant No. DGSR Ref. 2021-IRG-HBS-12.

Author contributions
M.A., A.A.K.H.I. and M.W. wrote the main manuscript text, M.A., M.S. and M.W. did the simulations and analysis, and M.A., A.A.K.H.I, M.S., A.A. and R.S. prepared figures and interpreted the results. All authors reviewed the manuscript.

Competing interests
The authors declare no competing interests.

Additional information
Correspondence and requests for materials should be addressed to A.H.I. or M.W.

Reprints and permissions information is available at www.nature.com/reprints.

Publisher's note Springer Nature remains neutral with regard to jurisdictional claims in published maps and institutional affiliations.